



# Bismuthene as a versatile photocatalyst operating under variable conditions for the photoredox C—H bond functionalization

Melek Sermin Ozer<sup>a,1</sup>, Zafer Eroglu<sup>a,e,1</sup>, Ahsen Sare Yalin<sup>a</sup>, Murat Kılıç<sup>b,\*</sup>,  
Ursula Rothlisberger<sup>b</sup>, Onder Metin<sup>a,c,d,\*\*</sup>

<sup>a</sup> Department of Chemistry, College of Sciences, Koç University, 34450 Istanbul, Turkey

<sup>b</sup> Laboratory of Computational Chemistry and Biochemistry, Institute of Chemical Sciences and Engineering, Ecole Polytechnique Fédérale de Lausanne, CH-1015 Lausanne, Switzerland

<sup>c</sup> Koç University Surface Science and Technology Center (KUYTAM), Istanbul 34450, Turkey

<sup>d</sup> Koç University TUPRAŞ Energy Center (KUTEM), Istanbul 34450, Turkey

<sup>e</sup> Division of Nanoscience and Nanoengineering, Institute of Natural and Applied Sciences, Atatürk University, 25240 Erzurum, Turkey

## ARTICLE INFO

### Keywords:

2D materials  
Bismuthene  
Photocatalyst  
Photoredox reaction  
C—H functionalization

## ABSTRACT

Recently, layered two-dimensional (2D) semiconductor materials composed of group 15 elements (pnictogens) are demonstrated as efficient photocatalysts in various applications. However, only little attention is given to the investigation of their catalytic properties, and even there is no example of the photocatalytic application of bismuthene so far. Here we report for the first time on the use of 2D bismuthene as a photocatalyst in a liquid-phase organic transformation. 2D bismuthene is proven to be an efficient photocatalyst that can be operated under various reaction conditions including indoor light illumination, darkness, outdoors and low temperature for the photoredox C—H arylation of (hetero)arenes with high product yields. The presented bismuthene catalyzed photoredox C—H arylation protocol works efficiently on a broad substrate scope of (hetero)arenes with aryl diazonium salts bearing electron-withdrawing and electron-donating groups. Moreover, a density functional theory (DFT) study reveals mechanistic details that lie behind the catalytic activity of bismuthene.

## 1. Introduction

Integration of photocatalysts that can use large portion of solar spectrum for chemical reactions is one of the most promising ways for making chemical transformations more efficient, environmentally friendly, sustainable, and economical, which are important targets in modern chemistry [1–3]. However, most of the conventional photocatalysts that have been used in various reactions so far are mostly activated by ultraviolet (UV) light or high-frequency visible light due to their large band gaps and suffer from low carrier mobility [4,5]. New semiconductor materials with proper band gap and high carrier mobility, which can be operated under low-frequency visible light or infrared light irradiation, or under daylight without any light source, are desired for photocatalytic applications. In recent years, layered 2D materials composed of group 15 elements (pnictogens) have attracted great attention in materials science owing to their extraordinary

electronic and optical properties that are beneficial for various applications [6–9]. As the monolayer of 2D pnictogens exhibits increased band gap with tunable electronic and optical properties, they are promising materials to be used as photocatalysts in different reactions. Among them, bismuthene, mono/few layer of 2D bismuth possessing excellent electron mobility properties [10], low toxicity [11], and high stability [12], exhibits unique potential for photocatalytic applications owing to its 2D hexagonal lattice, narrow band gap, and high surface area [13,14]. In addition to these favorable assets, bismuthene stands as a suitable photocatalytic material because it shows semiconducting properties with a tunable band gap of 0.3–1.0 eV when the exfoliated layers are thinner than 30 nm [15,16]. Despite its many advantageous properties as a possible photocatalyst, bismuthene has only been utilized as catalyst in electrochemical CO<sub>2</sub> reduction [17,18] and determination of lead and cadmium [19] so far. In addition to these electrocatalytic applications, a very recent paper reported that bismuthene could serve

\* Corresponding author.

\*\* Corresponding author at: Department of Chemistry, College of Sciences, Koç University, 34450 Istanbul, Turkey.

E-mail addresses: [murat.kilic@epfl.ch](mailto:murat.kilic@epfl.ch) (M. Kılıç), [ometin@ku.edu.tr](mailto:ometin@ku.edu.tr) (O. Metin).

<sup>1</sup> The authors contributed equally to this work.

as an electron mediator in carbon nitride/BiOCl heterojunction [20]. To the best of authors' knowledge, there is no example of using bismuthene as a photocatalyst in any liquid-phase chemical transformation so far.

Many efforts have been devoted to synthesizing arylated heteroarenes since they are crucial building blocks for the synthesis of complex organic molecules such as natural products and drugs [21–26]. To date, classical transition metal-catalyzed coupling partners including pre-activated (hetero)aryls have been used to form direct (hetero)aryl bonds, despite their very limited substrate scope [27,28]. However, the focus of research has recently shifted to the light-induced C–H functionalization after König's groundbreaking work on avoiding transition metal catalysts [29]. Consequently, with the motivation of a reduced number of reaction steps and milder reaction conditions, many researchers have contributed to the light-induced C–H functionalization by using various photocatalysts including transition metals [30–33], semiconductors [34–39], organic molecules [40–44], and others [45, 46]. Considering the advantages of this emerging field in synthetic organic chemistry, the direct functionalization of C–H bonds via photoredox catalysis is one of the most favorable pathways nowadays. The key point of the photoredox C–H functionalization is the generation of aryl radicals via single-electron transfer to a suitable substrate such as aryl diazonium salts. Even though aryl diazonium salts are the most investigated aryl radical precursors because of their mild reduction potentials [47,48], the selectivity of the late-stage complex molecules bearing other reducible groups under a given light energy in the presence of a photocatalyst should also be considered [49,50]. Many efficient photocatalysts have been reported for the photoredox C–H functionalization of different molecules with diazonium salts so far [25, 51]. However, since existing photoredox catalysts contain transition metals or organic molecules that have the recovery problem due to their intrinsic homogeneity and require external light sources and long reaction times to be activated, researchers have been trying to develop more efficient photocatalysts. Therefore, to expand the practical application of photoredox C–H functionalization, it is highly desirable to develop a low-cost and reusable photocatalyst that does not require a dry solvent, inert atmosphere, or even a light source to perform (photo) catalytic reactions in the context of green chemistry.

In this study, we report for the first time that a few-layered bismuthene is a versatile photoredox catalyst for the direct C–H arylation of (hetero)arenes. Unlike other photoredox catalysts tested in C–H arylation reactions so far, bismuthene can be operated, with high product yields reaching up to 98%, in a variety of ambient reaction conditions including indoor light irradiation, darkness, outdoors, and low temperature. A broad mechanistic study performed at various reaction conditions revealed that a photoredox process lies behind the catalytic activity of bismuthene. Moreover, the underlying mechanisms of the unprecedented activity of bismuthene in the C–H functionalization of arenes was elucidated by performing density functional theory calculations. Besides elucidating the catalytic nature of bismuthene via detailed mechanistic studies, this study also presents a large substrate scope for the application of bismuthene-based photoredox catalysis over a variety of heteroarenes (furan, thiophene and pyrrole) and, more importantly arenes (benzene and nitrobenzene) with aryl diazonium salts (total 43 examples) without using external light source under variety of ambient conditions. We believe that this study will open a new avenue in the photoredox catalysis, C–H functionalization, and 2D pnictogens for the development of more sustainable organic transformations.

## 2. Experimental

### 2.1. Materials

Bismuth (III) chloride ( $\text{BiCl}_3$ , 98+%), borane-*tert*-butylamine complex (TBAB, 97%), triethanolamine (TEOA), urea ( $\text{CH}_4\text{N}_2\text{O}$ ) (99%) and oleylamine (OAm, 70%) were obtained from Sigma-Aldrich. Red

phosphorus (98.9%), tin (99.5%), tin(IV) iodide (95%), *tert*-butyl nitrite (*t*-BuONO), tetrafluoroboric acid 50 wt% water ( $\text{HBF}_4$ ), acetonitrile (MeCN, 99.0%), and anilines were purchased from Alfa Aesar. Ethyl alcohol (EtOH, absolute, 99.9%), ethyl acetate ( $\text{EtOAc}$ ,  $\geq 99.5\%$ ), dimethyl sulfoxide (DMSO, 99.9%) dichloromethane (DCM,  $\geq 99.0\%$ ), *n*-hexane (96.0%), *N,N*-dimethylformamide (DMF, 99.0%), acetone (99.5%), and isopropyl alcohol (*i*-PrOH 99.5%), was purchased from IsoLab chemicals. *N*-methyl pyrrolidinone (NMP 99.8%) was obtained from Chemsolute. All chemicals and solvents were used as received without further purification unless it is noted.

### 2.2. Synthesis of bulk Bi and the preparation of bismuthene

$\text{BiCl}_3$  (1.0 mmol) was added into a 100 mL of four-necked round bottom flask with magnetic stirring bar under Argon flow as shown in Fig. S1. OAm (10.0 mL) was poured and stirred while it is attached to a continuous electronic temperature control via a thermocouple immersed in the solution and heated up to 120 °C. Then, the current Argon flow was stopped, right after replaced with vacuum controller and kept at this temperature for 30 min. Then TBAB (1.5 mmol) which dissolved in OAm (1.5 mL) via sonication was injected into the resulting  $\text{BiCl}_3$ -OAm solution. The mixed solution was stirred for 30 min at 120 °C and cooled naturally to room temperature. Finally, the resultant black precipitate was separated from the solution by centrifugation and washed with ethanol three times. The obtained powders were dried in a vacuum oven at 40 °C and then stored. Bulk bismuth was exfoliated in DMSO, DMF, EtOAc, NMP,  $\text{H}_2\text{O}$ , Acetone, *i*-PrOH, and MeCN under ambient conditions by ultrasonic homogenizer using a Bandelin Sonoplus 2200.2, 200 W, 25% amplitude, 1 h (Fig. S2).

### 2.3. Characterization

Scanning electron microscopy (SEM) images were taken with Zeiss Ultra Plus Field Emission Scanning Electron Microscope. Transmission electron microscopy (TEM), High angle annular dark field (HAADF) scanning transmission microscope (STEM) images and the associated EDS elemental mappings were conducted on a Hitachi HT7800 (TEM) with EXALENS (120 kV) working at high-resolution (HR) mode. Atomic force microscopy (AFM) measurements were carried out with using Bruker Dimension Icon AFM on the drop-cast flakes on high quality silicon wafer. Bruker D8 Advanced diffractometer (Cu K  $\alpha$  radiation, 1.54 Å) was recorded to generate XRD patterns. X-ray photoelectron spectroscopy (XPS) measurements were conducted on a Thermo Scientific X-ray photoelectron spectrometer with an aluminum anode (Al K $\alpha$ , 1468.3 eV). Raman spectra were carried out by using a Renishaw inVia Raman microscope (excitation source 532 nm) on Indium Tin Oxide (ITO) coated glass. UV–vis spectra were recorded on a Shimadzu 3600 Plus UV–Vis–NIR instrument. Photoluminescence spectroscopy (PL) data and time resolved photoluminescence spectroscopy (TRPL) of the materials were performed on an Edinburgh Instruments FLS1000 spectrometer (377 nm). Mott–Schottky analysis was taken with CHI 660e electrochemical workstation. As the working electrode, an ITO glass electrode was prepared by dropping 10  $\mu\text{L}$  of sample mixture (10 mg Bismuthene, 1000  $\mu\text{L}$ , IPA by ultrasonication) on the surface. And the reference electrode and the counter electrodes were Ag/AgCl (3 M KCl) and Pt wire, respectively while 0.5 M  $\text{Na}_2\text{SO}_4$  served as electrolyte. NMR spectra were recorded on Varian (operating at 500 MHz for  $^1\text{H}$  NMR) in  $\text{CDCl}_3$  with tetramethylsilane (TMS) as internal standard. Coupling constants (*J* values) are given in Hz and chemical shifts are reported parts per million (ppm). Splitting patterns are expressed as s (singlet), d (doublet), t (triplet), q (quartet), m (multiplet), and p (pentet). NMR spectra were processed with Bruker TopSpin 4.1.0 program. Column chromatography was performed by using thick walled glass columns and Silica Gel (Merck 60–200 mesh). Thin layer chromatography (TLC) Merck Silica Gel 60 F254) was performed by using commercially prepared 0.25 mm silica gel plates and visualization was provided by UV

lamp (254 nm). The relative proportions of solvents in chromatography solvent mixtures refer to the volume:volume ratio. GC-MS spectra were recorded on an Agilent Technologies 7890B GC-system with an Agilent 5977 A MSD HP-5 column (0.25 mm  $\times$  30 m, film: 0.25  $\mu$ m).

#### 2.4. General procedure for the photoredox C–H arylation

After the exfoliation of bulk bismuth in DMSO (1 mL), the corresponding mixture and the required heteroarene or arene were added to the 25 mL of jacketed flask with a stirring bar and a septum (Fig. S3a). Subsequently, the corresponding aryl diazonium salt (0.25 mmol) was added to the solution one pot as solid. The jacketed flask was kept at the required conditions (in light (Fig. S3b)/dark or with white light source (150 W) etc. detailed procedures in Supporting information). After 2 h of stirring the reaction mixture was transferred to separating funnel, diluted with DCM and washed with water (3  $\times$  10 mL). Then the organic layer was separated, dried over Na<sub>2</sub>SO<sub>4</sub>, filtered and concentrated. The residue was purified by column chromatography on SiO<sub>2</sub> using EtOAc/n-hexane as eluent if needed.

#### 2.5. Computational details

All Density Functional Theory (DFT) calculations were performed using the pw.x code of Quantum Espresso (v.6.6) [52]. The Generalized Gradient Approximation (GGA) to DFT in the Perdew–Burke–Ernzerhof (PBE) [53,54] formulation including dispersion corrections was used to optimize the atomic configurations and lattice parameters of a bismuthene nanosheet. Since standard semi-local DFT methods are not suitable for the calculation of the physisorption of aromatic compounds, the empirical correction (DFT-D3) proposed by Grimme et al. [55] was used for all DFT calculations. Ultrasoft pseudopotentials were used to describe the interaction between the (semi) valence and the core electrons for all of the atoms. Total electronic density and the Kohn–Sham orbitals were extended in a plane wave basis with 60 and 500 Ry energy cutoffs, respectively. A bismuthene 6 $\times$ 6 $\times$ 1 model containing 50

atoms under three-dimensional boundary conditions shown in Fig. 3 was used for all calculations. To decouple the 2D bismuthene nanosheet from its periodic replicas in the z-direction, a vacuum layer of 18 Å was used. The charge transfer analysis is carried out based on Bader [56] atoms in molecules method as implemented in the Bader v1.04 [57].

### 3. Results and discussion

#### 3.1. Synthesis and characterization of 2D bismuthene

To prepare bismuthene, firstly, layered bulk bismuth was synthesized by using a surfactant-assisted chemical reduction method in which bismuth (III) chloride (BiCl<sub>3</sub>) was reduced with borane-*tert*-butylamine complex in oleylamine (OAm) at 120 °C. In the protocol, OAm served both as surfactant and solvent. Next, bulk bismuth was exfoliated in different solvents with the ultrasonic probe homogenizer for 1 h to obtain a dark gray suspension of bismuthene nanosheets. The morphological, topological, and compositional features of as-prepared bismuthene were studied by using scanning electron microscopy (SEM), transmission electron microscopy (TEM), atomic force microscopy (AFM), and high-angle annular dark-field scanning transmission electron microscopy (HAADF-STEM) associated EDS elemental mapping. The SEM image of bismuthene confirmed the 2D layered flake-like structure at the nanoscale with lateral size of ca. 550 nm (Fig. 1a). The TEM image in Fig. 1b shows the ultrathin feature of bismuthene with the sub-micron lateral size. The AFM image and the associated height profile of bismuthene deposited on high quality silicon wafer (Fig. 1c and d) revealed that the yielded bismuthene had a 2D few-layer structure with a thickness of 4 nm, lateral size of 550 nm, and a smooth surface, all of which are consistent with the data acquired from TEM and SEM analysis. The low magnification HAADF-STEM image (Fig. 1e) and the associated EDS elemental mapping images of bismuthene (Fig. 1f and g) show that it composed of Bi atoms along with peddle O atoms attributed to surface oxidation as expected.

The crystal structure of layered bulk Bi was examined by powder X-

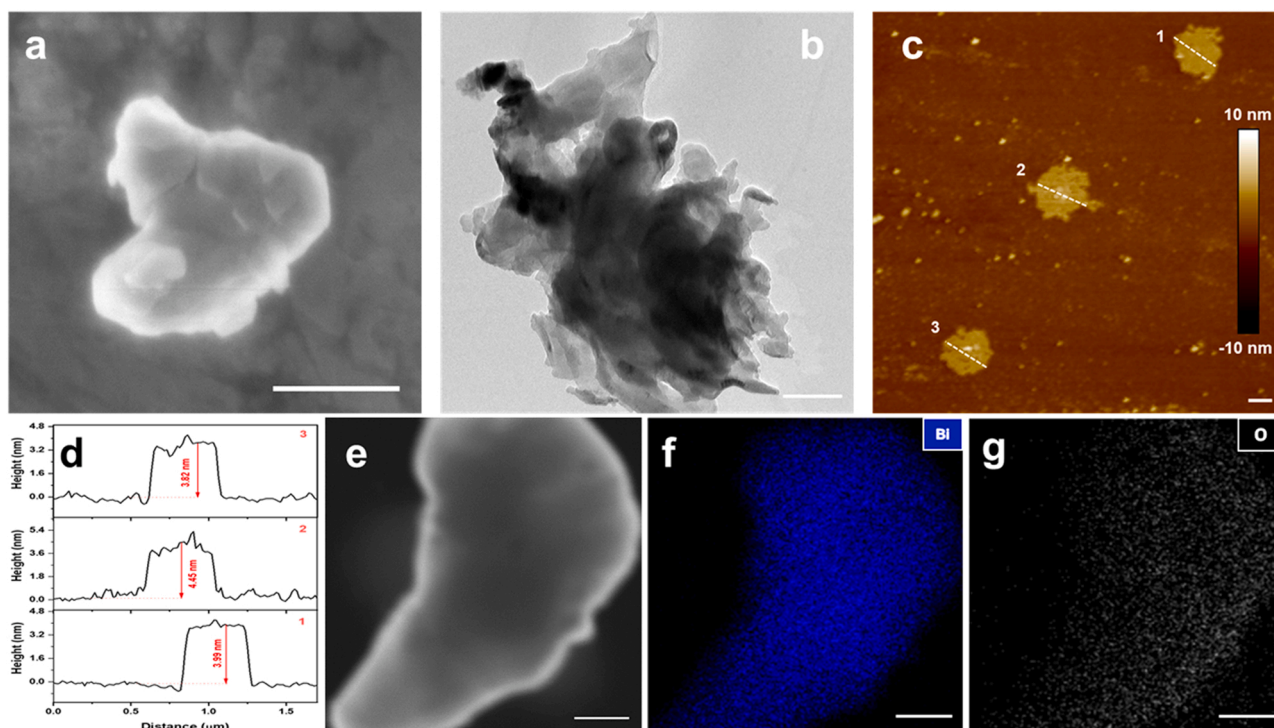


**Fig. 1.** a) SEM image of bismuthene b) TEM image of bismuthene. c) AFM image of bismuthene deposited on high quality silicon wafer. d) the corresponding height profiles for three bismuthene nanosheets marked in (c). e) Mott–Schottky plot of bismuthene. f) VB-XPS curves of bismuthene. g) O elemental mapping. Scale bars in figures (a, b, c, e, f and g) are all 200 nm.

ray diffraction (p-XRD). All the diffraction peaks observed in the p-XRD pattern of as-synthesized bulk Bi (Fig. 2a) are fully consistent with the rhombohedral bismuth (PDF no: 04-006-7762). It should be noted that there is no peak attributed to bismuth oxides ( $\alpha$ -Bi<sub>2</sub>O<sub>3</sub> or  $\beta$ -Bi<sub>2</sub>O<sub>3</sub>) observable in the pattern of bulk Bi, even after 60 days (Fig. S4a), indicating the stability of bulk Bi against oxidation to bismuth oxides under ambient conditions [17]. In Fig. 2b, to gain further insight about its surface chemical composition, bismuthene was analyzed with X-ray photoelectron spectroscopy (XPS). The XPS spectrum of Bi 4f core-level shows two doublets at binding energies (BE) of 157.6 and 162.8 eV, corresponding to the 4f<sub>5/2</sub> and 4f<sub>7/2</sub> core-levels of zerovalent Bi, respectively [7,12]. The high-resolution XPS spectrum of Bi 5d core-level of bismuthene (Fig. S5) also supported the existence of Bi(0). However, the large surface area of bismuthene made the surface oxidation inevitable during the sample preparation process for both of these analyses. No significant oxidation of Bi atoms was detected rather than the surface oxidation after 60 days period of time (Fig. S4b). The Raman spectrum of bismuthene showed two main peaks at 70.2 and 96.8 cm<sup>-1</sup>, which are attributed to the E<sub>g</sub> and A<sub>1g</sub> vibration modes of Bi(0), respectively (Fig. 2c) [12,18]. It should be noted that there is no peak assigned to bismuth oxides in the Raman spectra [12]. However, there is a clear shift to the higher wavenumber observable in both E<sub>g</sub> and A<sub>1g</sub> modes in the Raman spectrum of 2D bismuthene compared to the one for bulk Bi, indicating the decreased layer thickness thanks to the ultrasound-assisted liquid-phase exfoliation [17]. The visible-NIR absorption spectrum of bismuthene dispersed in dimethyl sulfoxide (DMSO) is presented in Fig. 2d in the range of 390–1600 nm. Based on the absorption spectrum, strong absorption peaks were observed at 1147, 1176, 1358, 1388, and 1486 nm, which are attributed to the layer-dependent optic-band gaps of bismuthene attached to the layers [58].

In order to define the capacitance of our material, the flat-band potential (E<sub>f</sub>) of bismuthene was determined by using the Mott–Schottky method. The results led us to construct the Mott–Schottky curve in Fig. 2e and accordingly, E<sub>f</sub> of bismuthene was calculated as −0.54 V

(Ag/AgCl, pH = 7). The conversion of the E<sub>f</sub> to the normal hydrogen electrode (NHE) potential is equal to −0.343 V (NHE, pH = 7) from the well-known equation ( $E_{\text{NHE}} = E_{\text{Ag/AgCl}} + 0.197$ ) [59]. The positive slope of the Mott–Schottky curve indicates that bismuthene is a n-type semiconductor. Based on the previous experimental observations in n-type semiconductors, while the value of E<sub>f</sub> was the same as the Fermi level, the CB potential was estimated to be 0.10 V more negative than that of E<sub>f</sub> [60,61]. As a result, the CB potential of bismuthene was found to be −0.443 eV. The VB potential of bismuthene was calculated as −0.05 eV from the VB-XPS spectrum of bismuthene (Fig. 2f). By using the formula of  $E_{\text{NHE}} = \phi + E_{\text{VB-XPS}} - 4.44$  ( $E_{\text{NHE}}$ : standard hydrogen electrode potential;  $\phi$ : electron work function of the XPS analyzer, the value was 4.543;  $E_{\text{VB-XPS}}$ : VB value was tested by VB-XPS), the VB edge potential of bismuthene was estimated to be 0.153 eV [62]. Overall, the band alignment of bismuthene can be schematically demonstrated as in Fig. S6. It can be concluded that ultrasound-assisted exfoliation process successfully converts semi-metallic layered bulk Bi to the few-layer bismuthene, resulting in semiconductor properties as reported in previous literature [63]. These new features of bismuthene clearly revealed that it could be used as a photocatalyst and pave a new path for different photocatalytic applications under visible or NIR light irradiation.

### 3.2. Bismuthene catalyzed photoredox C–H arylation

#### 3.2.1. Optimization experiments

The visible/NIR light-driven photocatalytic feature of bismuthene prompted us to investigate its photocatalytic activity in the photoredox C–H arylation of heteroarenes with diazonium salts to prepare (hetero) biaryl compounds under ambient conditions. Considering the photo-physical properties, band gap, and the edge potentials of few-layer bismuthene discussed above, furan **1a** and 4-chlorobenzenediazonium salt **2a** were selected as model compounds for conducting the optimization experiments in a jacketed glass reactor under indoor light illumination without using a light-source, and the results are depicted in Table 1. When the C–H arylation reaction was performed in DMSO by using

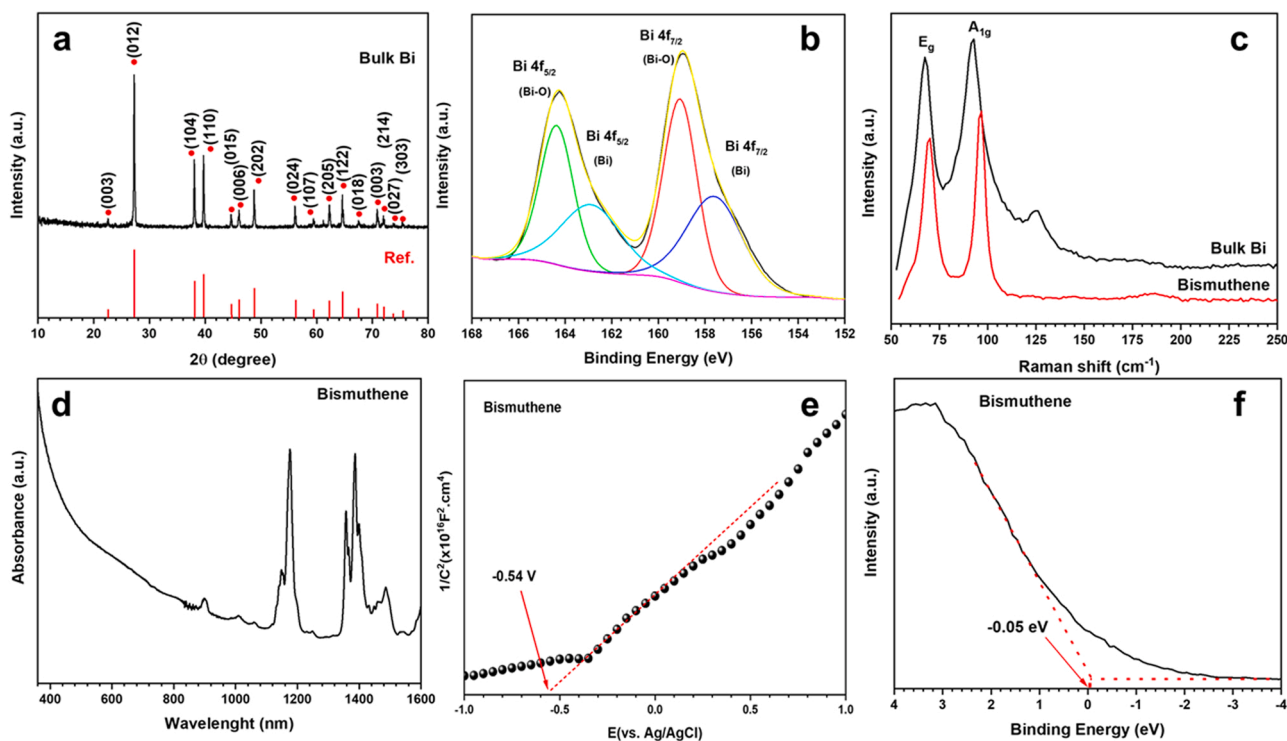


Fig. 2. a) XRD pattern of bulk Bi b) High-resolution XPS spectrum of Bi 4f core-level of bismuthene c) Raman spectrum of bulk Bi and bismuthene deposited on ITO d) Vis-NIR absorption spectrum of bismuthene in DMSO e) The Tauc plot of bismuthene f) Mott–Schottky plot of bismuthene.

**Table 1**

Optimization of the reaction conditions for bismuthene catalyzed photoredox C–H arylation of heteroarenes.

Entry	Conditions <sup>a</sup>	Yield[%] <sup>b</sup>
1	<b>1a</b> (10 equiv), DMSO, 25 °C	63
2	<b>1a</b> (20 equiv), DMSO, 25 °C	75, 67 <sup>c</sup> , 77 <sup>d</sup>
3	<b>1a</b> (50 equiv), DMSO, 25 °C	84, 80 <sup>e</sup>
4	<b>1a</b> (20 equiv), DMF, MeCN, NMP, H <sub>2</sub> O, Acetone, 25 °C	45, 38, 14, 25, Trace
5	<b>1a</b> (20 equiv), DMSO, 25 °C, 5 mg catalyst	69
6	<b>1a</b> (20 equiv), DMSO, 25 °C, no catalyst	Trace
7	<b>1a</b> (20 equiv), DMSO, 25 °C, bulk Bi	36
8	<b>1a</b> (20 equiv), DMSO, 25 °C, DARK <sup>f</sup>	76
9	<b>1a</b> (20 equiv), DMSO, 5 °C	76
10	<b>1a</b> (20 equiv), DMSO, 5 °C, DARK <sup>f</sup>	75

<sup>a</sup> All reactions were carried out with 10 mg catalyst on a scale of 5 mmol of **1a** and 0.25 mmol of **2a** in 1 mL of solvent at 25 °C under indoor light irradiation for 2 h unless otherwise noted.

<sup>b</sup> Yields were determined by <sup>1</sup>H NMR analysis with 1,3-dinitrobenzene as internal standard.

<sup>c</sup> Reaction time is 1 h.

<sup>d</sup> Reaction time is 4 h.

<sup>e</sup> Isolated yield.

<sup>f</sup> The reaction flask was covered with aluminum foil and the reaction was performed in a closed box in dark.

different equiv. of **1a**, the desired product **3a** was obtained in the highest yield of 84% (Table 1, entry 1–3) in the presence of 50 equiv. of **1a**. These outcomes were consistent with the fact that preventing the homocoupling of generated aryl intermediates depends on the concentration of heteroarenes as reported [36]. In addition, lowering the amount of **1a** results in the formation of bisfunctionalized product. However, since the yield of the C–H arylation reaction where 20 equiv. of **1a** (75%) was used is very close to the one obtained by using 50 equiv. of **1a**, we decided to use 20 equiv. of **1a**. To exhibit the effect of solvents in the catalytic activity of bismuthene in the C–H arylation reactions, different solvents such as *N,N*-dimethylformamide (DMF), acetonitrile (MeCN), *N*-methyl-pyrrolidine (NMP), water and acetone were examined (Table 1, entry 4). The highest yield was achieved in DMSO which is reported to be an appropriate solvent for the photocatalytic reactions [29,40]. After deciding DMSO as the solvent, we turned our attention to other reaction parameters including catalyst amount, reaction time and temperature. The variables in these reaction parameters did not result in remarkable enhancement in the product yield (Table 1, entries 1–5). For example, only 3% and 8% increments were observed in the product yield with prolonging the reaction time from 2 h to 4 h (Table 1, entry 3). On the other hand, the yield was dropped to 69% when the catalyst amount decreased to 5 mg while no product was obtained in the absence of catalyst (Table 1, entry 5–6).

In view of the yield variations under these conditions, we continued the other optimization experiments with 10 mg of bismuthene. On the other hand, non-exfoliated bulk Bi provided only 36% yield and the product yield increased with prolonging sonication time, which was a clear and convincing evidence for the requirement of well-dispersed bismuthene nanosheets for efficient photoredox catalysis (Table 1, entry 7). To our delight, there was no drop observed in the product yield when the reaction was conducted in dark at 25 °C and 5 °C (Table 1, entry 8–10). Upon these results, it can be concluded that no additional light source and elevated temperature is needed for the photocatalytic activation of bismuthene owing to its narrow band gap, which can be

regarded as a superior result when compared to earlier literature (Table S1). With these interesting and exciting results, we dived with into the catalytic nature of bismuthene by studying some mechanistic experiments before exploring substrate scope.

### 3.2.2. Mechanistic studies

To propose a plausible reaction mechanism for the presented intriguing photocatalytic activity of bismuthene, we turned our attention to two main experimental studies. Both results depicted in Table 1 (entries 8–10) revealing the effect of the light/temperature on the photocatalytic activity of bismuthene and typical scavenger experiments will help us to propose a proper reaction mechanism. Considering the possible excitation of bismuthene under indoor lighting owing to its narrow band gap (0.60 eV), various experiments have been conducted to understand how the yields alter under a given light at different conditions. First, we aimed to unveil the optoelectronic features of bismuthene by eliminating the effect of temperature and thus decided to change our solvent from DMSO to DMF due its relatively lower freezing point. When the bismuthene catalyzed photoredox C–H arylation was performed at 5 °C under indoor light, the yield was dramatically dropped and only a trace amount of product **3a** was obtained (for comparison see Fig. 3a, entries 1, 4). No product formation was even detected when lowering the temperature to –15 °C (Fig. 3a, entry 7). With the results of these two experiments in hand, performing the same reaction under a light source (white light), the product yield jumped to 72% (Fig. 3a, entries 8–9), which affirms the photocatalytic nature of the reaction mechanism. Second, 1,4-benzoquinone (BQ) was used as sacrificial electron acceptor to understand whether single-electron was transferred from the activation of bismuthene under indoor light illumination. The observation of a dramatic decrease in the product yield from 84% to 12% in the presence of BQ indicate that excited electrons have a crucial role in the reaction mechanism. In addition, when triethanolamine (TEOA) was added to the reaction mixture as a hole scavenger, the product yield was also decreased to 25%. These results provide obvious sign for the reaction mechanism in which the electron transfer to the holes of bismuthene is the key factor in the formation of the major active species. Both excited electrons and holes generated on the conduction band (CB) and valence band (VB) of bismuthene, respectively, are involved in the photocatalytic reaction mechanism. Moreover, using 2,2,6,6-tetramethylpiperidinoxyl (TEMPO) as a radical scavenger further confirmed the formation of the aryl radical species by capturing the active intermediate and lowering the product (**3a**) yield to 14% (Fig. 3b). In addition to all these results, another experimental proof supporting the proposed reaction mechanism was the higher product yield provided by bismuthene compared to that of bulk Bi. The electron charge carriers that are generated by bismuthene nanosheets under a light illumination and the deceleration of recombination even at low temperatures and dark (Table 1, entries 2, 8–10) might be the reason the product formation quantitatively equal that of indoor light conditions. To summarize, properties such as large surface area, unique electronic mobility, and layered structure with tunable bandgap of a semiconductor are required since the reaction occurs via SET mechanism.

Both the steady-state photoluminescence (PL) and time-resolved photoluminescence (TRPL) analyses were performed to better understand the relation of bismuthene and substrates (Fig. S7). As compared to bismuthene, the PL intensity in the experiments including diazonium salt **2a** and bismuthene were greatly decreased. This can be interpreted by the more efficient migration of electrons from bismuthene to **2a** substrate for the generation of aryl radical as shown in Fig. 3c. TRPL studies along with PL results are consistent with the fast migration of photogenerated electrons since the average lifetimes in bismuthene are shorter than that of bismuthene in the presence of diazonium salts [64, 65]. In the light of these results, a plausible reaction mechanism is proposed in Fig. 3c.

In the proposed mechanism, the low band gap of bismuthene nanosheets enables their excitation under indoor light/cold or dark/cold. The

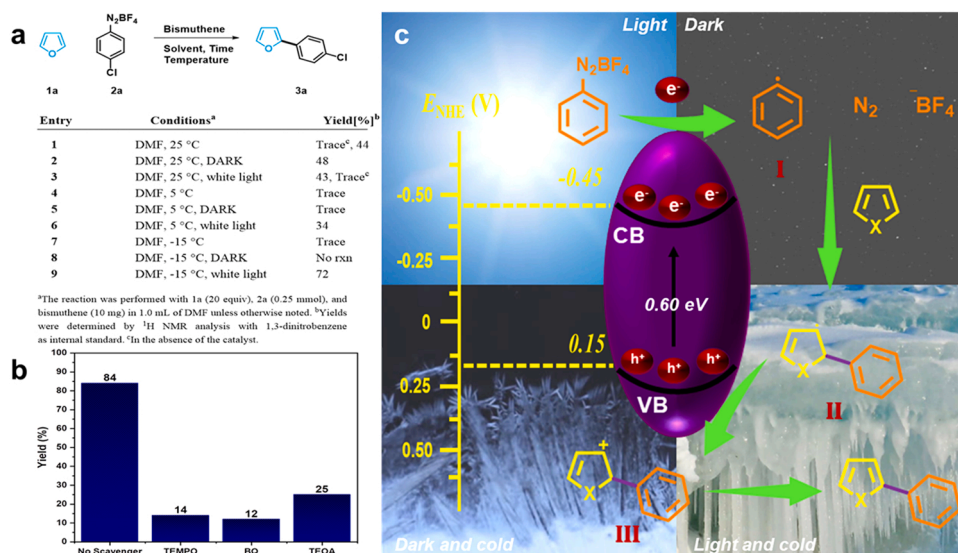


Fig. 3. a) Temperature/light experiments and the effect of the light. b) scavenger experiments. c) plausible reaction mechanism.

excited electron on the CB of bismuthene is transferred to the aryl diazonium salt and aryl radical is generated and followed by the addition of I to the corresponding heteroarene to give the intermediate II. The electron transfer from II to the valence band of bismuthene resulted in the oxidized cation III. Radical chain propagation might be alternative to oxidize the intermediate II to III when 1a reduces to I, however, this pathway was eliminated since the decrease in the yield of the hole scavenger experiment (Fig. 3b). Last but not the least, the deprotonation of III produces the final compound 3a. One of the most important advantageous of heterogeneous catalyst is being reusable for a certain period of time.

The reusability of bismuthene as a heterogeneous photoredox catalyst was evaluated in the C–H arylation of 4-nitrobenzenediazonium salt and furan (1a) and the results were depicted in Fig. S8. There was almost no decrease observed in the product yield up to the 3rd successive run and 95% product yield was obtained at the end of 3rd catalytic run. However, a slight decrease in the product yield to 75% and 73% was observed in the 4th and 5th run, respectively. To understand the decrease in the product yield after the 5th run, the crystal structure and morphology of the recovered bismuthene were characterized by XRD, TEM and STEM-HAADF EDS mapping. XRD pattern of bismuthene after the 5th catalytic run revealed that there were new peaks appeared in addition to the major peaks of rhombohedral bismuth indicating the oxidation of bismuthene. Additionally, TEM and EDS elemental mapping images depicted in Fig. S8c–f indicated that the morphology and size of bismuthene nanosheets has changed after the 5th run. Therefore, the decrease observed in the product yield after the 5th run might be attributed to the changes both in the photophysical properties of bismuthene due to the formation of bismuth oxides and in the surface properties and 2D structure. These results indicate that further studies are needed to improve the stability of bismuthene, which are under investigation in our group.

After clarifying mechanism of these transformation as well as the other advantages of the presented bismuthene catalyzed photoredox C–H arylation protocol, such as dispensing with the need for inert atmosphere, degassing, base, etc., the substrate scope was investigated by using 10 mg of exfoliated bismuthene nanosheets, in the presence of heteroarene at 25 °C under indoor light illumination.

### 3.2.3. Substrate scope and limitations

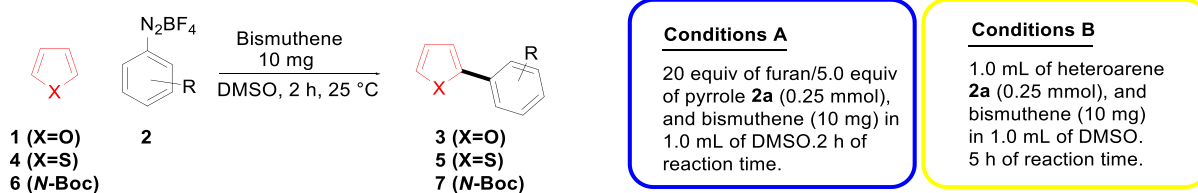
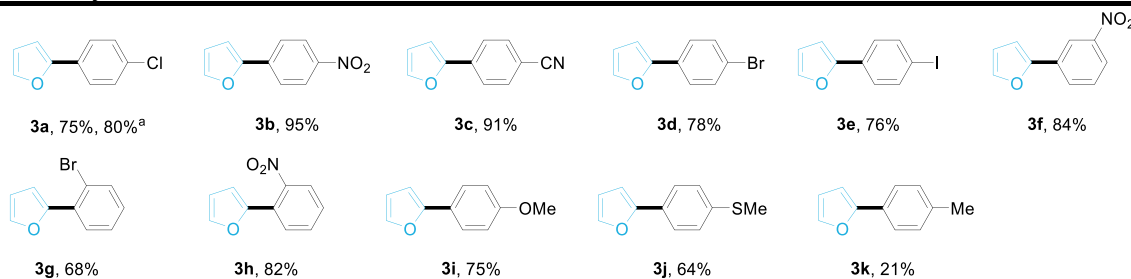
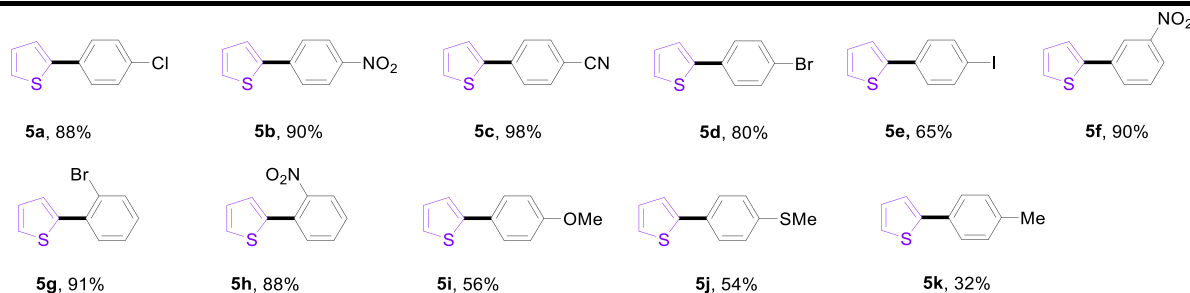
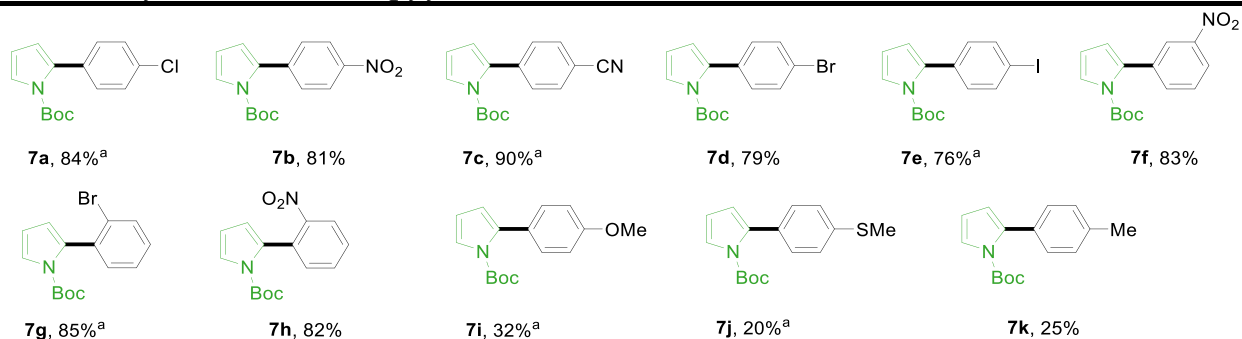
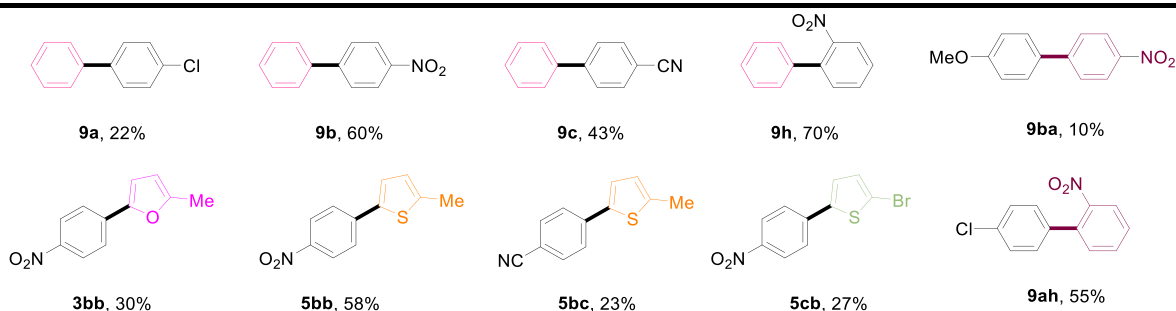
With the optimum reaction conditions and mechanistic study in hand, the substrate scope, and limitations of bismuthene catalyzed photoredox C–H arylation reactions were explored over different

(hetero)arenes and aryl diazonium salts bearing electron-withdrawing (EWG) and electron-donating (ED) groups having different reduction potentials (Table 2). It is worth noting once more that the presented photoredox C–H arylation protocol does not require any complicated reaction setup, light source, inert atmosphere, and degassed solvents. Firstly, the reaction furan and diazonium salt derivatives bearing EWG attached to para-position of diazonium salts (Table 2, part a, 3a–3e) resulted in good to excellent yields in the range of 76–95%. When ortho-substituted aryl diazonium salts were used as substrate, the corresponding products (Table 2, part a, 3g and 3h) were obtained in 68% and 82% yields, respectively. After screening the possible steric hindrance of the ortho-substituted aryl diazonium salts and achieving a yield 84% of the desired product 3f, the ones bearing ED groups (–SMe, –OMe) produced 3i and 3j in good yields (75% and 64%).

Even though bismuthene could tolerate halogens and convert the ED attached aryl diazonium salts to desired products in good yields, –Me substituted and unsubstituted products resulted in trace amounts (Table 2, part a). These results encouraged us to increase the amount of 1a to 50 equiv. and yet 3k was still obtained in a low yield (21%). All these outcomes clearly show that the comparatively challenging –Me substituted and unsubstituted aryl diazonium salts are the limitations of the presented bismuthene catalyzed photocatalytic C–H arylations.

To widen the applicability of the presented protocol, other heteroarenes including thiophene and pyrrole were tested as well as arenes and other substituted heteroarenes. In the case of thiophenes, we had to slightly alter the optimized reaction conditions due to the low product yields (Table S3). For example, the use of an external light source doubling the yield, then the increase in the equiv. of thiophene and prolonging the reaction time (5 h) elevated the yield of 5a up to 88% (Table 2, part b). After these small modifications, the products 5a–5k were obtained in moderate to excellent yields (Table 2, part b). When the optimized conditions used in the photoredox C–H arylation of furan were applied to the pyrroles, the desired C–H arylated products 7a–7k were obtained in moderate to good yields (Table 2, part c). A similar trend was observed for the yields of para-, meta- and ortho-substituted diazonium salts with thiophene or pyrrole as of furan. It is especially noteworthy that the products 3e, 5e, and 7e were successfully yielded under the presented photocatalytic conditions. Other photocatalysts might not provide this selectivity because of the lower reduction potential of Ar–I compared to other aryl halides [66]. As a result, it can be speculated that bismuthene catalyzed photoredox reactions can be utilized to build up C–C bonds selectively in complex structures with light-sensitive molecules such as aryls bearing iodine. However, there is

Table 2

Scope and limitation of diazonium salts **2** in the bismuthene catalyzed photoredox C–H arylation of various heteroarenes and arenes.<sup>a</sup> Condition B was followed.**a. C–H arylation of furan under condition A****b. C–H arylation of thiophene under condition B****c. C–H arylation of N-Boc pyrrole under condition A****d. C–H arylation of arenes and other heteroarenes under condition B**

only a limited number of examples for the photoredox C–H arylation of arenes since it is a more challenging process than that of heteroarenes [67]. For instance, most of the well-known photoredox catalysts, such as König's Eosin Y, could not yield the desired biaryl product from the C–H arylation of arenes [29,68]. To date, the C–H arylation of arenes has only been achieved by using precious metal catalysts [31] or other unsustainable catalysts [26,42,43]. In this regard, we decided to test the bismuthene catalyzed photoredox C–H arylation on arenes by taking benzene as a model compound. We were delighted to observe that the C–H arylation of benzene with 4-chlorodiazonium salt (**2a**) resulted in the related biaryl product with 22% yield, which was a good hint for the further improvement of the reaction conditions and for studying benzene with other diazonium salts. The successful transformations are shown in Table 2, part d. The longer reaction time did not help to improve the yield, yet poor to moderate yields of 22%, 60%, 43% and 70% were obtained for the products **9a–9c** and **9h**, respectively (Table 2, part d). It should be noted that the yields of the biaryl products were consistent with the reduction potential of the diazonium salts [47, 48]. At this point, it can be hypothesized that the possible interaction of arenes with the surface of the bismuthene might have a key role in their activation for the nucleophilic addition of aryl radical formed by diazonium salt.

To prove this claim and study the interaction of bismuthene with arenes, DFT calculations were performed on a model monolayer bismuthene with a surface-adsorbed benzene molecule (Fig. 4). First, the most stable adsorption position of benzene on the monolayer bismuthene surface was determined on the basis of Perdew-Burke-Ernzerhof (PBE) functional including dispersion corrections (DFT-D3) by placing the benzene molecule on different adsorption sites and orientations. Adsorption energies  $E_{\text{ads}}$  were calculated by using the following expression:  $E_{\text{ads}} = E_{\text{tot}} - (E_{\text{surface}} + E_{\text{adsorbate}})$ . For the energetically most stable system,  $E_{\text{ads}}$  was calculated to be  $-29$  kJ/mol for benzene lying flat on top of one of the bismuth atoms in the bismuthene model surface. Possible charge transfer between benzene and the bismuthene surface that could promote substrate activation was investigated on the basis of a Bader charge analysis. According to the results of this analysis (Table S8), there is an effective charge difference between the adsorbed system and the single components, indicating that there is a partial electron transfer ( $0.04 e^-$ ) from bismuthene to the substrate. Although significant, the amount of charge transfer is comparable with one reported for other systems like benzene on Ag(100) ( $0.03 e^-$ ) and Cu(110) ( $0.07 e^-$ ) [69]. The band gap of the monolayer bismuthene was calculated to be  $0.65$  eV which in good agreement with the experimental value ( $0.60$  eV). As a result of the DFT studies, it can be concluded that bismuthene reveals a unique property compared to conventional

photoredox catalysts since it already promotes a partial charge transfer to the aromatic substrate in the electronic ground state in agreement with the sustained catalytic activity in the dark while the magnitude of charge transfer can be further increased via photoexcitation.

Next, we turned our attention to other substituted heteroarenes and arenes to see the regioselectivity under these reaction conditions. As suggested by the DFT studies, the C–H arylation of nitrobenzene was studied to support the possible partial electron transfer from bismuthene to arene rings. The probable electron transfer of bismuthene to nitrobenzene was tested with ED (–OMe) and EWD (–Cl) attached two different diazonium salts (Table 2, part d). The selected nitrobenzene in photocatalyzed C–H arylation as a radical trap has been avoided up to now due to its electron deficiency and non-selectivity. To the best of authors' knowledge, the very-first trial of nitrobenzene-arylation was successful and experimentally confirmed the possibility of partial electron transfer to make the electron deficient arene capture the aryl radical. Even though the selectivity was poor and ortho-para- arylation of nitrobenzene occurred, the yielded products **9ba** (10%) and **9ah** (55%) was another proof of a radical mechanism. While **3bb** was formed in 30% of the yield as the only regio-isomer as shown in the literature [29], the other tested heteroarenes resulted in the predominantly 2-substituted products **5bb**, **5 bc**, and **5cb** along with minor 3-substituted isomers. Additional experiments were carried out to compare the reactivity difference between the diazonium salts (Fig. S9). A notable competition was observed and electron poor diazonium salt predominantly reacted with heteroarenes. This result led us to investigate the intermolecular competition between heteroarene and arene (Fig. S10). 4-chlorobenzenediazonium salt preferentially reacted with furan (**1a**) and no significant product was formed with benzene. C–H arylation of heteroarenes and arenes with bismuthene was compatible with light-sensitive functional groups and a broad substrate scope. Due to mild conditions bismuthene catalyzed photoredox C–H arylation can be preferred for structures including different aryl moieties based on these optimized conditions and competition experiments.

#### 4. Conclusions

In conclusion, few-layer bismuthene nanosheets were successfully prepared from the exfoliation of bulk Bi, which was synthesized by using a new method comprising a surfactant-assisted chemical reduction of bismuth(III) chloride. The yielded bismuthene nanosheets dispersed in DMSO solvent were used as a photoredox catalyst for the C–H arylation of (hetero)arenes with diazonium salts. As far as we know, this is the first example of photocatalytic application of bismuthene not only in organic synthesis but also in a liquid-phase chemical reaction. To our delight,

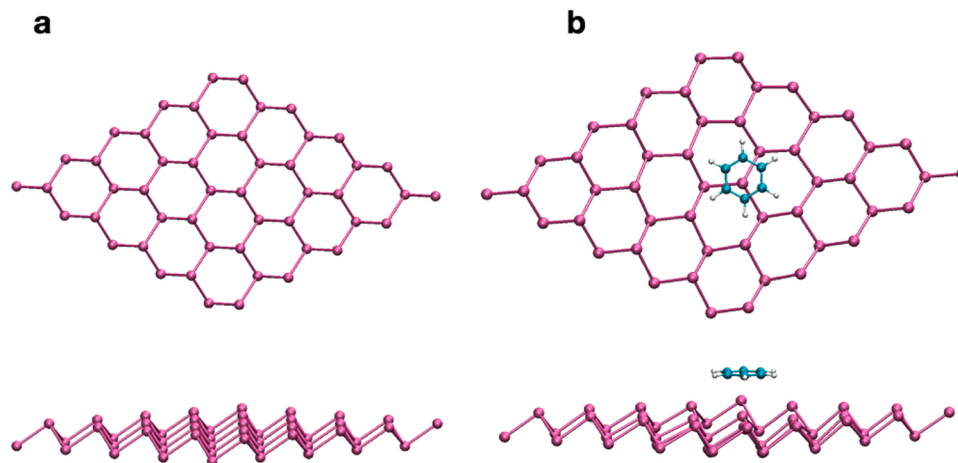


**Fig. 4.** a) Optimized model structure of monolayer bismuthene, b) optimized position of benzene on bismuthene viewed from y-direction (up) and from z-direction (down). Purple, cyan and gray spheres represent Bi, C and H atoms, respectively.

bismuthene showed high catalytic activity in the C–H arylation of heteroarenes such as furan, thiophene, pyrrole, and, more importantly, benzene with aryl diazonium salts under indoor light illumination without using a light source or darkness at room temperature or low temperatures. Additionally, our DFT studies showed a partial charge transfer from bismuthene to the surface-adsorbed substrate. The structural characterization of bismuthene was consistent with the intriguing photoredox activity in the studied C–H arylation reactions. The lack of need for a light source and temperature-independent photocatalysis ability of bismuthene is the first example of the photoredox C–H functionalization and thus has a high potential to open a new avenue in organic synthesis. Moreover, this study can expand the list of potential photocatalytic applications of bismuthene.

## CRediT authorship contribution statement

**Melek Sermin Ozer:** Conceptualization, Formal analysis, Methodology, Validation, Investigation, Writing – original draft, Visualization. **Zafer Eroglu:** Conceptualization, Formal analysis, Methodology, Validation, Investigation, Writing – original draft, Visualization. **Ahsen Sare Yalin:** Methodology, Investigation. **Murat Kilic:** Methodology, Software, Formal analysis, Data curation, Writing – original draft. **Ursula Rothlisberger:** Supervision, Writing – review & editing, Funding acquisition, Provision. **Onder Metin:** Conceptualization, Writing – review & editing, Supervision, Funding acquisition, Project administration, Validation, Provision.

## Declaration of Competing Interest

The authors declare that they have no known competing financial interests or personal relationships that could have appeared to influence the work reported in this paper.

## Acknowledgments

Ö.M. thanks to The Turkish Academy of Sciences (TUBA) for the financial support. Z.E. thanks to the Council of Higher Education (YOK) and The Scientific and Technological Research Council of Turkey (TUBİTAK) for the Ph.D. scholarship (YOK/100-2000 and TUBİTAK 2211-C). M.K. and U.R. acknowledge HPC resources of CSCS (Swiss National Supercomputer Centre).

## Appendix A. Supporting information

Supplementary data associated with this article can be found in the online version at [doi:10.1016/j.apcatb.2021.120957](https://doi.org/10.1016/j.apcatb.2021.120957).

## References

- [1] I. Ghosh, J. Khamrai, A. Savateev, N. Shlapakov, M. Antonietti, B. König, Organic semiconductor photocatalyst can bifunctionalize arenes and heteroarenes, *Science* 365 (2019) 360–366, <https://doi.org/10.1126/science.aaw3254>.
- [2] E. Swift, A durable semiconductor photocatalyst, *Science* 365 (2019) 320–321, <https://doi.org/10.1126/science.aax8940>.
- [3] L.X. Chen, Z.W. Chen, M. Jiang, Z. Lu, C. Gao, G. Cai, C.V. Singh, Insights on the dual role of two-dimensional materials as catalysts and supports for energy and environmental catalysis, *J. Mater. Chem. A* 9 (2021) 2018–2042, <https://doi.org/10.1039/D0TA08649E>.
- [4] R. Feng, W. Lei, G. Liu, M. Liu, Visible- and NIR-light responsive black-phosphorus-based nanostructures in solar fuel production and environmental remediation, *Adv. Mater.* 30 (2018) 1–9, <https://doi.org/10.1002/adma.201804770>.
- [5] M. Zhu, S. Kim, L. Mao, M. Fujitsuka, J. Zhang, X. Wang, T. Majima, Metal-free photocatalyst for H<sub>2</sub> evolution in visible to near-infrared region: black phosphorus/graphitic carbon nitride, *J. Am. Chem. Soc.* 139 (2017) 13234–13242, <https://doi.org/10.1021/jacs.7b08416>.
- [6] M. Pumera, Z. Sofer, 2D monoelemental arsenene, antimonene, and bismuthene: beyond black phosphorus, *Adv. Mater.* 29 (2017), 1605299, <https://doi.org/10.1002/adma.201605299>.
- [7] C.C. Mayorga-Martinez, R. Gusmão, Z. Sofer, M. Pumera, Soft-based enzymatic phenol biosensors: phosphorene, arsenene, antimonene, and bismuthene, *Angew. Chem. Int. Ed.* 58 (2018) 134–138, <https://doi.org/10.1002/anie.201808846>.
- [8] S. Zhang, S. Guo, Z. Chen, Y. Wang, H. Gao, J. Gómez-Herrero, P. Ares, F. Zamora, Z. Zhu, H. Zeng, Recent progress in 2D group-VA semiconductors: from theory to experiment, *Chem. Soc. Rev.* 47 (2018) 982, <https://doi.org/10.1039/C7CS00125H>.
- [9] S. Zhang, M. Xie, F. Li, Z. Yan, Y. Li, E. Kan, W. Liu, Z. Chen, H. Zeng, Semiconducting group 15 monolayers: a broad range of band gaps and high carrier mobilities, *Angew. Chem. Int. Ed.* 55 (2016) 1666–1669, <https://doi.org/10.1002/anie.201507568>.
- [10] X. Liu, S. Zhang, S. Guo, B. Cai, S.A. Yang, F. Shan, M. Pumera, H. Zeng, Advances of 2D bismuth in energy sciences, *Chem. Soc. Rev.* 49 (2020) 263, <https://doi.org/10.1039/C9CS00551J>.
- [11] J. Zhou, J. Chen, M. Chen, J. Wang, X. Liu, B. Wei, Z. Wang, J. Li, L. Gu, Q. Zhang, H. Wang, L. Guo, Few-layer bismuthene with anisotropic expansion for high-area-capacity sodium-ion batteries, *Adv. Mater.* 31 (2019), 1807874, <https://doi.org/10.1002/adma.201807874>.
- [12] J. Zhang, S. Ye, Y. Sun, F. Zhou, J. Song, J. Qu, Soft-template assisted synthesis of hexagonal antimonene and bismuthene in colloidal solutions, *Nanoscale* 12 (2020) 20945, <https://doi.org/10.1039/D0NR05578F>.
- [13] T. Chai, X. Li, T. Feng, P. Guo, Y. Song, Y. Chen, H. Zhang, Few-layer bismuthene for ultrashort pulse generation in a dissipative system based on an evanescent field, *Nanoscale* 10 (2018) 17617, <https://doi.org/10.1039/C8NR03068E>.
- [14] W. Huang, J. Zhu, M. Wang, L. Hu, Y. Tang, Y. Shu, Z. Xie, H. Zhang, Emerging mono-elemental bismuth nanostructures: controlled synthesis and their versatile applications, *Adv. Funct. Mater.* 31 (2020), 2007584, <https://doi.org/10.1002/adfm.202007584>.
- [15] E.S. Walker, S.R. Na, D. Jung, S.D. March, J.-S. Kim, T. Trivedi, W. Li, L. Tao, M. L. Lee, K.M. Liechti, D. Akinwande, S.R. Bank, Large-area dry transfer of single-crystalline epitaxial bismuth thin films, *Nano Lett.* 16 (2016) 6931–6938, <https://doi.org/10.1021/acs.nanolett.6b02931>.
- [16] S.M. Beladi-Mousavi, Y. Ying, J. Plutnar, M. Pumera, Bismuthene metallurgy: transformation of bismuth particles to ultrahigh-aspect-ratio 2D microsheets, *Small* 16 (2020), 2002037, <https://doi.org/10.1002/sml.202002037>.
- [17] W. Zhang, Y. Hu, L. Ma, G. Zhu, P. Zhao, X. Xue, R. Chen, S. Yang, J. Ma, J. Liu, Z. Jin, Liquid-phase exfoliated ultrathin Bi nanosheets: Uncovering the origins of enhanced electrocatalytic CO<sub>2</sub> reduction on two-dimensional metal nanostructure, *Nano Energy* 53 (2018) 808–816, <https://doi.org/10.1016/j.nanoen.2018.09.053>.
- [18] F. Yang, A. Elnabawy, O.R. Schimmenti, P. Song, J. Wang, Z. Peng, S. Yao, R. Deng, S. Song, Y. Lin, M. Mavrikakis, W. Xu, Bismuthene for highly efficient carbon dioxide electroreduction reaction, *Nat. Commun.* 11 (2020) 2352, <https://doi.org/10.1038/s41467-020-14914-9>.
- [19] A.C. Lazanas, K. Tsirka, A.S. Paipetis, M.I. Prodromidis, 2D bismuthene/graphene modified electrodes for the ultra-sensitive stripping voltammetric determination of lead and cadmium, *Electrochim. Acta* 336 (2020), 135726, <https://doi.org/10.1016/j.electacta.2020.135726>.
- [20] D. Zhang, X. Cui, L. Liu, Y. Xu, J. Zhao, J. Han, W. Zheng, 2D bismuthene metal electron mediator engineering super interfacial charge transfer for efficient photocatalytic reduction of carbon dioxide, *ACS Appl. Mater. Interfaces* 13 (2021) 21582–21592, <https://doi.org/10.1021/acsaami.1c01470>.
- [21] F.-X. Felpin, S. Sengupta, Biaryl synthesis with arenediazonium salts: crosscoupling, CH-arylation and annulation reactions, *Chem. Soc. Rev.* 48 (2019) 1150–1193, <https://doi.org/10.1039/C8CS00453F>.
- [22] X. Zhang, Y. Mei, Y. Li, J. Hu, D. Huang, Y. Bi, Visible light-mediated functionalization of aryl diazonium salts, *Asian J. Org. Chem.* 10 (2021) 453–463, <https://doi.org/10.1002/ajoc.202000636>.
- [23] D. Kozjakov, G. Wu, A.J. von Wangelin, Aromatic substitutions of arenediazonium salts via metal catalysis, single electron transfer, and weak base mediation, *Org. Biomol. Chem.* 16 (2018) 4942–4953, <https://doi.org/10.1039/C8OB00591E>.
- [24] X.-Y. Yu, J.-R. Chen, W.-J. Xiao, Visible light-driven radical-mediated C–C bond cleavage/functionalization in organic synthesis, *Chem. Rev.* 121 (2021) 506–561, <https://doi.org/10.1021/acs.chemrev.0c00030>.
- [25] S.S. Babu, P. Muthuraja, P. Yadav, P. Gopinath, Aryldiazonium salts in photoredox catalysis – recent trends, *Adv. Synth. Catal.* 363 (2021) 1782–1809, <https://doi.org/10.1002/adsc.202100136>.
- [26] R. Saritha, S.B. Annes, S. Saravanan, S. Ramesh, Carbazole based electron donor acceptor (EDA) catalysis for the synthesis of biaryl and aryl–heteroaryl compounds, *Org. Biomol. Chem.* 18 (2020) 2510–2515, <https://doi.org/10.1039/D0OB00282H>.
- [27] L.-C. Campeau, N. Hazari, Cross-coupling and related reactions: connecting past success to the development of new reactions for the future, *Organometallics* 38 (2019) 3–35, <https://doi.org/10.1021/acs.organomet.8b00720>.
- [28] A. Tlahuext-Aca, S.Y. Lee, S. Sakamoto, J.F. Hartwig, Direct arylation of simple arenes with aryl bromides by synergistic silver and palladium catalysis, *ACS Catal.* 11 (2021) 1430–1434, <https://doi.org/10.1021/acscatal.0c05254>.
- [29] D.P. Hari, P. Schroll, B. König, Metal-free, visible-light-mediated direct C–H arylation of heteroarenes with aryl diazonium salts, *J. Am. Chem. Soc.* 134 (2012) 2958–2961, <https://doi.org/10.1021/ja212099r>.
- [30] Y.-F. Liang, R. Steinbock, L. Yang, L. Ackermann, Continuous visible-light photoflow approach for a manganese catalyzed (Het)arene C–H arylation, *Angew. Chem. Int. Ed.* 57 (2018) 10625–10629, <https://doi.org/10.1002/anie.201805644>.
- [31] S. Chakraborty, J. Ahmed, B.K. Shaw, A. Jose, S.K. Mandal, An iron-based long-lived catalyst for direct C–H arylation of arenes and heteroarenes, *Chem. Eur. J.* 24 (2018) 17651–17655, <https://doi.org/10.1002/chem.201803402>.
- [32] S. Dixit, Q.T. Siddiqui, M. Muneer, N. Agarwal, Ferrocene catalysed C–H arylation of arenes and reaction mechanism study using cyclic voltammetry, *Tetrahedron Lett.* 57 (2016) 4228–4231, <https://doi.org/10.1016/j.tetlet.2016.08.020>.

- [33] V. Gauchot, D.R. Sutherland, A.-L. Lee, Dual gold and photoredox catalysed C–H activation of arenes for aryl–aryl cross couplings, *Chem. Sci.* 8 (2017) 2885, <https://doi.org/10.1039/C6SC05469B>.
- [34] E. Kalay, H. Küçükkeçeci, H. Kilic, Ö. Metin, Black phosphorus as a metal-free, visible-light-active heterogeneous photoredox catalyst for the direct C–H arylation of heteroarenes, *Chem. Commun.* 56 (2020) 5901–5904, <https://doi.org/10.1039/DOCC01874K>.
- [35] L. Zhi, H. Zhang, Z. Yang, W. Liu, B. Wang, Interface coassembly of mesoporous MoS<sub>2</sub> based-frameworks for enhanced near-infrared light driven photocatalysis, *Chem. Commun.* 52 (2016) 6431, <https://doi.org/10.1039/C6CC00780E>.
- [36] T. Amaya, D. Hata, T. Moriuchi, T. Hirao, Polyaniline-induced C–H arylation of arenes with arenediazonium salts, *Chem. Eur. J.* 21 (2015) 16427–16433, <https://doi.org/10.1002/chem.201501969>.
- [37] X. Cai, H. Liu, L. Zhi, H. Wen, A. Yu, L. Li, F. Chen, B. Wang, A g-C<sub>3</sub>N<sub>4</sub>/rGO nanocomposite as a highly efficient metal-free photocatalyst for direct C–H arylation under visible light irradiation, *RSC Adv.* 7 (2017) 46132, <https://doi.org/10.1039/C7RA07462J>.
- [38] X. Cao, T. Han, Q. Peng, C. Chen, Y. Li, Modifications of heterogeneous photocatalysts for hydrocarbon C–H bond activation and selective conversion, *Chem. Commun.* 56 (2020) 13918–13932, <https://doi.org/10.1039/D0CC05785A>.
- [39] J. Liu, H. Wang, J. Bai, T. Li, Y. Yang, Y. Peng, B. Wang, Gram-scale synthesis of aligned C<sub>3</sub>N<sub>4</sub>-polypyrrole heterojunction aerogels with tunable band structures as efficient visible and near infrared light-driven metal-free photocatalysts, *J. Mater. Chem. A* 5 (2017) 24920–24928, <https://doi.org/10.1039/C7TA08389K>.
- [40] E. Tatumashvili, B. Chan, P.E. Nashar, C.S.P. McElean,  $\sigma$ -Bond initiated generation of aryl radicals from aryl diazonium salts, *Org. Biomol. Chem.* 18 (2020) 1812–1819, <https://doi.org/10.1039/D0OB00205D>.
- [41] S.B. Annes, S. Ramesh, 1,3,5-Triphenylpyrazoline-based organocatalysis: synthesis of aryl-heteroaryl compounds and exploiting by-product from the reaction for alkyne-carbonyl metathesis (ACM) reaction in one pot, *Asian J. Org. Chem.* (2019) 1398–1404, <https://doi.org/10.1002/ajoc.201900305>.
- [42] J. Ahmed, S. Chakraborty, A.S. Jose, S.K. Mandal, Integrating organic lewis acid and redox catalysis: the phenalenyl cation in dual role, *J. Am. Chem. Soc.* 140 (2018) 8330–8339, <https://doi.org/10.1021/jacs.8b04786>.
- [43] M.D. Perretti, D.M. Monzón, F.P. Crisóstomo, V.S. Martín, R. Carrillo, Radical C–H arylations of (hetero)arenes catalyzed by gallic acid, *Chem. Commun.* 52 (2016) 9036–9039, <https://doi.org/10.1039/C5CC09911K>.
- [44] S. Zhang, Z. Tang, W. Bao, J. Li, B. Guo, S. Huang, Y. Zhang, Y. Rao, Perylenequinoid-catalyzed photoredox activation for the direct arylation of (het) arenes with sunlight, *Org. Biomol. Chem.* 17 (2019) 4364–4369, <https://doi.org/10.1039/C9OB00659A>.
- [45] M. Tavakolian, M. Hosseini-Sarvari, Catalyst-free organic transformations under visible-light, *ACS Sustain. Chem. Eng.* 9 (2021) 4296–4323, <https://doi.org/10.1021/acssuschemeng.0c06657>.
- [46] Y.-S. Feng, X.-S. Bu, B. Huang, C. Rong, J.-J. Dai, J. Xu, H.-J. Xu, NADH coenzyme model compound as photocatalyst for the direct arylation of (hetero)arenes, *Tetrahedron Lett.* 58 (2017) 1939–1942, <https://doi.org/10.1016/j.tetlet.2017.04.001>.
- [47] C. Galli, Radical reactions of arenediazonium ions: an easy entry into the chemistry of the aryl radical, *Chem. Rev.* 88 (1988) 765–792, <https://doi.org/10.1021/cr00087a004>.
- [48] F.F. Gadallah, R.M. Eloffson, Arylation of aromatic compounds by electrochemical reduction of benzenediazonium tetrafluoroborate in aprotic solvents, *J. Org. Chem.* 34 (1969) 3335–3338, <https://doi.org/10.1021/jo01263a025>.
- [49] S. Gisbertz, B. Pieber, Heterogeneous photocatalysis in organic synthesis, *ChemPhotoChem* 4 (2020) 456–475, <https://doi.org/10.1002/cptc.202000014>.
- [50] I. Ghosh, L. Marzo, A. Das, R. Shaikh, B. König, Visible light mediated photoredox catalytic arylation reactions, *Acc. Chem. Res.* 49 (2016) 1566–1577, <https://doi.org/10.1021/acs.accounts.6b00229>.
- [51] F. Mo, D. Qui, L. Zhang, Recent development of aryl diazonium chemistry for the derivatization of aromatic compounds, *Chem. Rev.* 121 (2021) 5741–5829, <https://doi.org/10.1021/acs.chemrev.0c01030>.
- [52] P. Giannozzi, S. Baroni, N. Bonini, M. Calandra, R. Car, C. Cavazzoni, D. Ceresoli, G.L. Chiarotti, M. Cococcioni, I. Dabo, A.D. Corso, S. de Gironcoli, S. Fabris, G. Fratesi, R. Gebauer, U. Gerstmann, C. Gougousis, A. Kokalj, M. Lazzeri, L. Martin-Samos, N. Marzari, F. Mauri, R. Mazzarello, S. Paolini, A. Pasquarello, L. Paulatto, C. Sbraccia, S. Scandolo, G. Sclauzero, A.P. Seitsonen, A. Smogunov, P. Umari, R.M. Wentzcovitch, QUANTUM ESPRESSO: a modular and open-source software project for quantum simulations of materials, *J. Phys. Condens. Matter* 21 (2009), 395502, <https://doi.org/10.1088/0953-8984/21/39/395502>.
- [53] J.P. Perdew, K. Burke, Y. Wang, Generalized gradient approximation for the exchange-correlation hole of a many-electron system, *Phys. Rev. B* 54 (1996) 16533–16539, <https://doi.org/10.1103/PhysRevB.54.16533>.
- [54] J.P. Perdew, K. Burke, M. Ernzerhof, Generalized gradient approximation made simple, *Phys. Rev. Lett.* 77 (1996) 3865–3868, <https://doi.org/10.1103/PhysRevLett.77.3865>.
- [55] R.F.W. Bader, *Atoms in Molecules: A Quantum Theory*, Oxford University Press, New York, 1990.
- [56] S. Grimme, J. Antony, S. Ehrlich, H. Krieg, A consistent and accurate ab initio parametrization of density functional dispersion correction (DFT-D) for the 94 elements H–Pu, *J. Chem. Phys.* 132 (2010), 154104, <https://doi.org/10.1063/1.3382344>.
- [57] G. Henkelman, A. Arnaldsson, H. Jónsson, A fast and robust algorithm for Bader decomposition of charge density, *Comput. Mater. Sci.* 36 (2006) 354–360, <https://doi.org/10.1016/j.commatsci.2005.04.010>.
- [58] L. Lu, Z. Liang, L. Wu, Y.X. Chen, Y. Song, S.C. Dhanabalan, J.S. Ponraj, B. Dong, Y. Xiang, F. Xing, D. Fan, H. Zhang, Few-layer bismuthene: sonochemical exfoliation, nonlinear optics and applications for ultrafast photonics with enhanced stability, *Laser Photonics Rev.* 12 (2018), 1700221, <https://doi.org/10.1002/lpor.201700221>.
- [59] S. Lian, Z. Wang, Q. Sun, Y. Tang, L. Liu, H. Wang, Z. Wang, Q. Wu, Enhanced CH<sub>4</sub> selectivity in CO<sub>2</sub> photocatalytic reduction over carbon quantum dots decorated and oxygen doping g-C<sub>3</sub>N<sub>4</sub>, *Nano Res.* 12 (2019) 2749–2759, <https://doi.org/10.1007/s12274-019-2509-2>.
- [60] Q.-Q. Yang, R.-T. Liu, C. Huang, Y.-F. Huang, L.-F. Gao, B. Sun, Z.-P. Huang, L. Zhang, C.-X. Hu, Z.-Q. Zhang, C.-L. Sun, Q. Wang, Y.-L. Tang, H.-L. Zhang, 2D bismuthene fabricated via acid-intercalated exfoliation showing strong nonlinear near-infrared responses for mode-locking lasers, *Nanoscale* 10 (2018) 21106, <https://doi.org/10.1039/C8NR06797J>.
- [61] T. Zhang, J. Yu, J. Huang, S. Lan, Y. Lou, J. Chen, MoC/MAPbI<sub>3</sub> hybrid composites for efficient photocatalytic hydrogen evolution, *Dalton Trans.* 50 (2021) 10860, <https://doi.org/10.1039/D1DT01809D>.
- [62] J. Xiong, X. Li, J. Huang, X. Gao, Z. Chen, J. Liu, H. Li, B. Kang, W. Yao, Y. Zhu, CN/rGO@BPQDs high-low junctions with stretching spatial charge separation ability for photocatalytic degradation and H<sub>2</sub>O<sub>2</sub> production, *Appl. Catal. B Environ.* 266 (2020), 118602, <https://doi.org/10.1016/j.apcatb.2020.118602>.
- [63] K. Noda, Y. Igarashi, H. Imai, Y. Oaki, Yield-prediction models for efficient exfoliation of soft layered materials into nanosheets, *Chem. Commun.* 57 (2021) 5921, <https://doi.org/10.1039/D1CC01440D>.
- [64] F. Chen, T. Ma, T. Zhang, Y. Zhang, H. Huang, Atomic-level charge separation strategies in semiconductor-based photocatalysts, *Adv. Mater.* 33 (2021), 2005256, <https://doi.org/10.1002/adma.202005256>.
- [65] C. Han, Y.-H. Li, J.-Y. Li, M.-Y. Qi, Z.-R. Tang, Y.-J. Xu, Cooperative syngas production and C–N bond formation in one photoredox cycle, *Angew. Chem. Int. Ed.* 60 (2021) 7962–7970, <https://doi.org/10.1002/anie.202015756>.
- [66] I. Ghosh, T. Ghosh, J.I. Bardagi, B. König, Reduction of aryl halides by consecutive visible light-induced electron transfer processes, *Science* 346 (2014) 725–728, <https://doi.org/10.1126/science.1258232>.
- [67] P.K. Vardhanapu, J. Ahmed, A. Jose, B.K. Shaw, T.K. Sen, A.A. Mathews, S. K. Mandal, Phenalenyl based aluminum compound for catalytic C–H arylation of arene and heteroarenes at room temperature, *J. Org. Chem.* 84 (2019) 289–299, <https://doi.org/10.1021/acs.joc.8b02699>.
- [68] K. Kubota, Y. Pang, A. Miura, H. Ito, Redox reactions of small organic molecules using ball milling and piezoelectric materials, *Science* 366 (2019) 1500–1504, <https://doi.org/10.1126/science.aay8224>.
- [69] W. Reckien, M. Eggers, T. Bredow, Theoretical study of the adsorption of benzene on coinage metals, *Beilstein J. Org. Chem.* 10 (2014) 1775–1784, <https://doi.org/10.3762/bjoc.10.185>.